Partial carbonization and etching of ZIF-9 to construct SO2-4decorated C@NiCoFe LDH ultrathin nanosheets for efficient oxygen evolution reaction

Weibin Chen, Chao Chen, Lei Li *, Zhan Lin *

Guangdong Provincial Key Laboratory of Plant Resources Biorefinery, School of Chemical Engineering and Light Industry, Guangdong University of Technology, Guangzhou 510006, China

*Corresponding authors. *E-mail address*: li.lei@gdut.edu.cn, zhanlin@gdut.edu.cn

Experimental Section

Chemicals. Benzimidazole (H-PhIM), cobalt acetate tetrahydrate ($Co(CH_3COO)_2 \cdot 4H_2O$), nickel nitrate hexahydrate ($Ni(NO_3)_2 \cdot 6H_2O$), ferrous sulfate heptahydrate ($FeSO_4 \cdot 7H_2O$), ferrous chloride ($FeCl_2$), ferrous acetate tetrahydrate ($Fe(CH_3COO)_2 \cdot 4H_2O$), potassium hydroxide (KOH), N, N-dimethylformamide (DMF), ethanol and methanol were purchased from Aladdin Reagents. Iridium oxide (IrO_2) and Ir/C (20%) were obtained from Premetek. Nafion (5 wt%) solution was acquired from Alfa Aesar. All reagents and solvents were used as received without further purification, and the water used in all experiments was purified to >18.25 MΩ cm^{-1} by a Millipore sigma instrument.

Synthesis of C@ZIF-9 precursor

Typically, 2.4908 g $Co(CH_3COO)_2 \cdot 4H_2O$ and 2.3628 g H-PhIM were successively dissolved in a mixed solution containing 100 mL methanol and 100 mL DMF. After stirring for 6 h, the mixture was centrifuged and the obtained deposit was washed repeatedly with methanol. The product was dried at 80 °C for 10 h. After that, the obtained ZIF-9 powder was annealed at 500 °C for 240 min under N_2 atmosphere.

Synthesis of C@NiCoFe LDH

80 mg C@ZIF-9 was dispersed in 50 mL ethanol (solution A). 160 mg $Ni(NO_3)_2 \cdot 6H_2O$ and 0.18 mmol ferrous salt ($FeSO_4 \cdot 7H_2O$, $Fe(CH_3COO)_2 \cdot 4H_2O$, or $FeCl_2$) were dissolved in 5 mL water (solution B). Solution A and B were mixed together, and refluxed at 90 °C for 60 min. Precipitate were collected by centrifugation, washed with absolute ethanol, and air-dry at 60 °C for 10 h. For convenience, the final

products were denoted as C@NiCoFe-SO_4, C@NiCoFe-OAc, and C@NiCoFe-Cl, respectively.

For comparison, the NiCoFe-SO_4, NiCoFe-OAc, and NiCoFe-Cl were also fabricated using a similar way, except that the C@ZIF-9 precursor was replaced by ZIF-9 precursor.

Synthesis of C@NiCo LDH and NiCo LDH

The synthesis of C@NiCo LDH was similar to that of C@NiCoFe-x (x= SO_4, OAc and Cl) without adding ferrous salt.

The synthesis of NiCo LDH was similar to that of C@NiCo LDH, except that the C@ZIF-9 precursor was substituted by ZIF-9 precursor.

Characterizations of catalysts

X-ray diffraction (XRD) was performed on a Bruker D8 Advanced X-ray Diffractometer with Cu-Ka radiation (λ = 0.15406 nm). Infrared spectroscopy was obtained in Nicolet IS50 fourier transform infrared (FT-IR) spectrum with the range of 500 - 4000 cm^{-1}. The morphological structure of the catalysts was investigated by scanning electron microscope (SEM, TESCAN MIRA LMS) and transmission electron microscopy (TEM, JEOL-JEM 2100 F). X-ray photoelectron spectroscopy (XPS) patterns were obtained using a Thermo Scientific K-Alpha instrument with Al-Kα radiation (*hv* = 1486.6 eV). The Brunauer-Emmett-Teller (BET) specific surface area was determined by a N_2 adsorption-desorption analyzer (ASAP2020) at 77 K, and the Barrett-Joyner-Halenda (BJH) method was used to analyze pore size distributions. In-situ Raman spectra and Raman spectra were recorded using a Raman system (HORIBA LabRAM) with a 532 nm laser source wavelength. The thickness was tested by atomic force microscopy (AFM) using a Bruker Dimension Icon. The mass loading of nickel, cobalt and iron were determined by inductively coupled plasma mass spectrometer (ICP-MS, Agilent 7700s).

Electrochemical measurements

All the electrochemical measurements were carried out on a CHI-760E electrochemical workstation at ambient temperature (~25 ^oC). The catalysts modified a glassy carbon rotating disk electrode (GCE, effective geometric area: 0.196 cm^2) was utilized as the working electrode, while a Hg/HgO (1.0 M KOH) and a platinum wire

were employed as the reference and the counter electrode, respectively. To prepare working electrode, approximately 2 mg of catalyst was dispersed in a mixture solution containing 250 μL ethanol, 100 μL water and 20 μL Nafion (5 wt %), followed by sonication at least 30 min. Then, the 20 μL of resulting homogeneous dispersion was dropped onto the GCE. Linear sweep voltammetry (LSV) curves were tested at the rotation speed of 1,600 rpm in an O_2-saturated 0.1 M KOH electrolyte with a scan rate of 5 mV·s^{-1}. Before recording the catalytic activity, the working electrode was activated by twenty segments Cyclic Voltammetry (CV). Electrochemical impedance spectroscopy (EIS) measurements were performed under 0.62 V from 1,000 kHz to 0.1 Hz. The long-term stability test for OER was conducted through the Chronoamperometry (CP) measurement at 10 mA cm^{-2} and CV tests for 2,000 cycles. To evaluate the electric double-layer capacitance (C_{dl}), CVs were tested in 0.2 - 0.3 V ranging from 60 to 160 mV s^{-1}. And the electrochemically active surface area (ECSA) can be calculated as: ECSA = C_{dl}/C_s (C_s = 0.040 mF cm^{-2}). The overall water splitting experiment in 1.0 M KOH was conducted in a two-electrode cell with the C@NiCoFe-SO_4(+)||Pt/C(-) coupled catalyst. All the potentials in this study were converted to the reversible hydrogen electrode (RHE) through the Nernst equation with 90% IR-compensation: E (*vs.* RHE) = E (*vs*. Hg/HgO) + 0.059×pH + 0.098 - 90% IR_s, where the I and R_s represent the current and the ohmic drop tested by impedance spectroscopy, respectively.

Turnover frequency (TOF) values were calculated from the equation [1]:

$$TOF = \frac{j * A}{4 * F * m}$$

Where j, A, F and m represent the current density at a specific potential, the surface area of the electrode, the Faraday constant (96485 C mol^{-1}) and the number of moles of active materials loaded on the working electrode, respectively. All the Ni, Co and Fe atoms in the catalysts are assumed as active sites.

Faradic efficiency was calculated from the ratio of the recorded gas volume to the theoretical gas volume during the charge passed through the electrode. The formula was listed below [1]:

$$Faradaic\ yield = \frac{V_{experimental}}{V_{theoretical}} = \frac{V_{experimental}}{\frac{1}{4} \times \frac{Q}{F} \times V_m}$$

In which the Q, F, and V_m represent the charge passed through the electrode, the Faraday constant (96485 C mol^{-1}), and the molar volume of gas (24.5 L mol^{-1}, 298 K, 101 kPa), repectively. The number 4 means 4-mol electrons per mole O_2.

Density Functional Theory (DFT) Calculation

All calculations were performed according to the first-principles using Perdew-Burke-Ernzerhof (PBE) formulation with spin-polarized density functional theory (DFT) methods within the generalized gradient approximation (GGA) [2,3,4]. The projected augmented wave (PAW) potential was chosen to describe the ionic cores, and the plane wave cutoff energy was set to be 450 eV [5,6]. The DFT-D3 scheme proposed by Grimme was adopted to describe the van der Waals interactions [7,8]. The electronic energy was set as self-consistent when the energy change was smaller than 10-5 eV, while a geometry optimization was considered as convergent with the energy change less than 0.02 eV $Å^{-1}$. Gamma centered (1 × 1 × 1) Brillouin zone was used during the relaxation. To eliminate the artificial interactions between periodic images, the surface was normally added with 15 Å vacuum layer. Spin polarized calculations were carried out for this calculation. To calculate Gibbs free energy of oxygen evolution reaction, the computational hydrogen electrode (CHE) model developed by Nørskov et al. was employed to build the adsorption model [9]. The free energy change (ΔG) is defined as follow: $\Delta G = \Delta E + \Delta E_{zpe} - T\Delta S + \Delta G_{pH}$ - eU, where ΔE, ΔE_{zpe} and ΔS are stand for the difference of total energy, zero-point energy, and entropy between products and reactants for all elementary reactions in four-electrons OER procedure, respectively. The value of ΔG_{pH} (pH=13) is determined as 0.769 eV according to $\Delta G_{pH} = -kBT\ln[H^+]$. U and e are presented as the electrode potential and transferred charge, respectively. The NIST database was considered as reference to obtain the entropies of the free molecule H_2O [10]. Meanwhile, because of the bad description of magnetism of O_2 in VASP, the free energy of O_2 can be obtained according to the equation of $G(O_2) = 4.92 + 2G(H_2O) - 2(H_2)$.

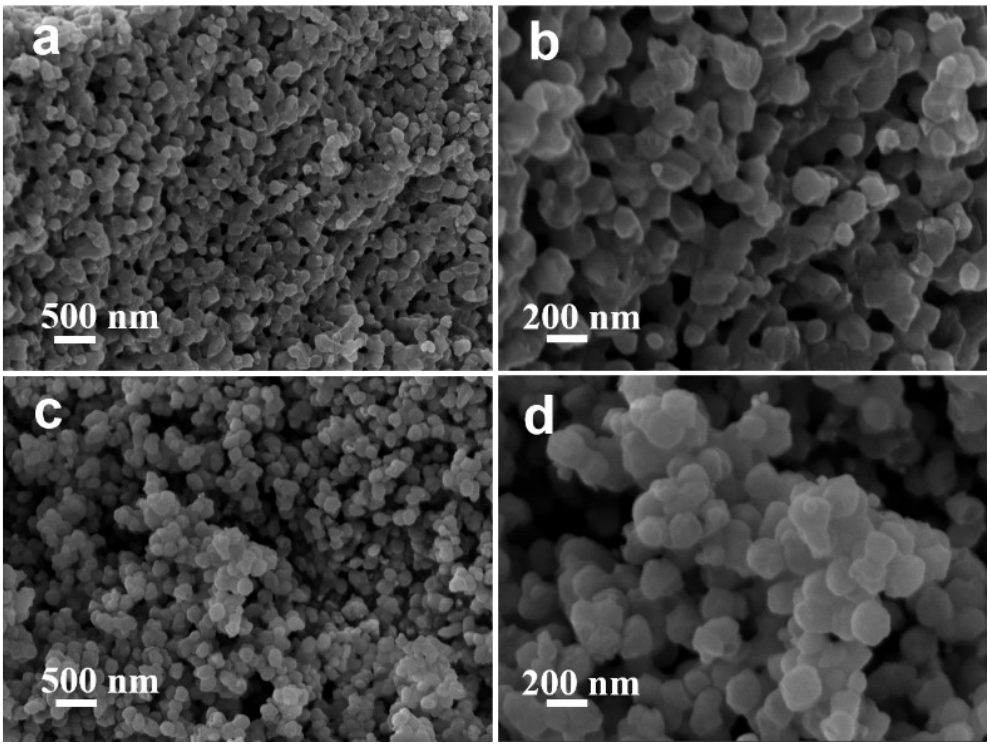

Figure S1. SEM images of (a,b) ZIF-9 and (c,d) C@ZIF-9.

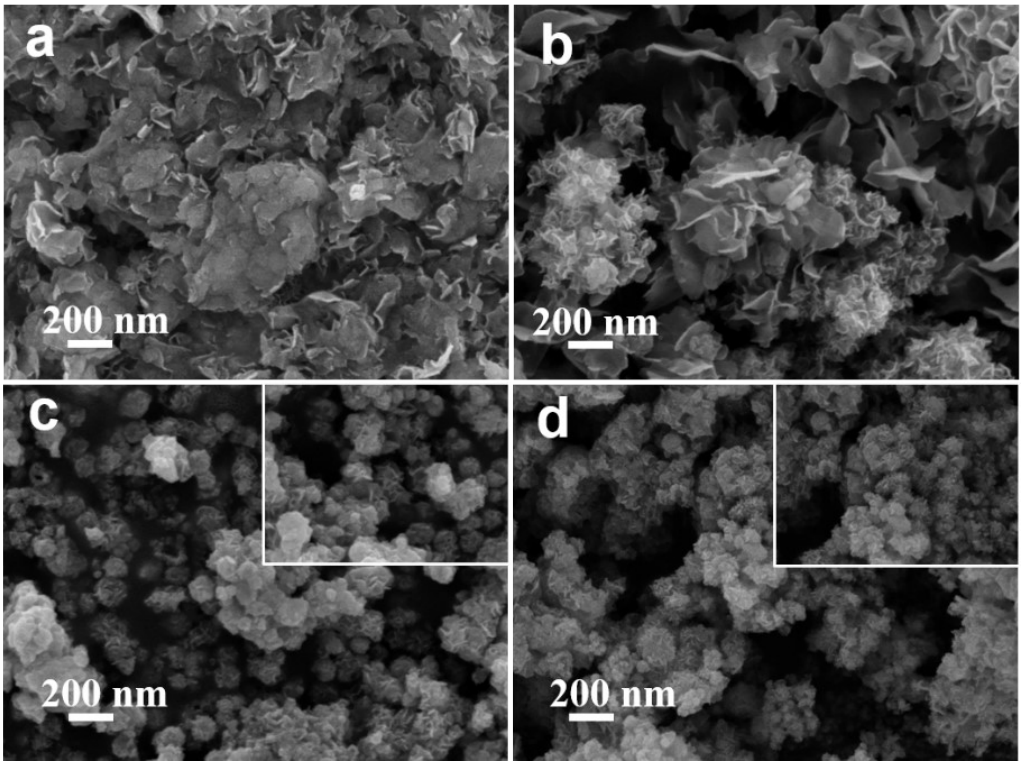

Figure S2. SEM images of (a) NiCo LDH, (b) C@NiCo LDH, (c) NiCoFe-SO_4, and (d) C@NiCoFe-SO_4.

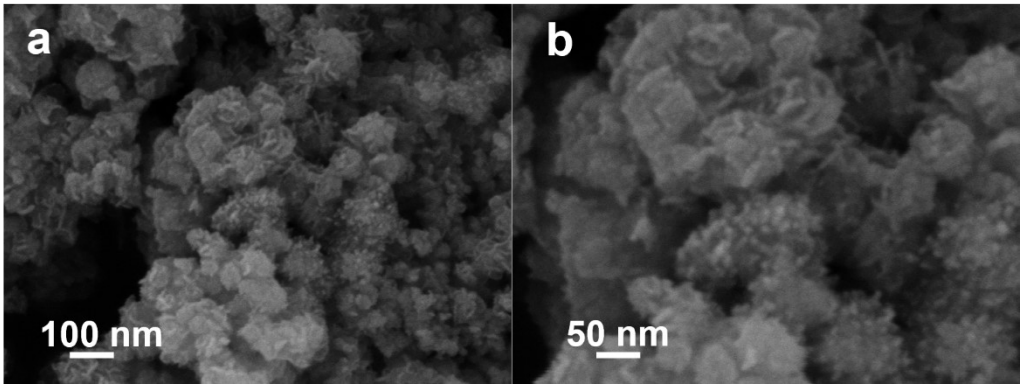

Figure S3. High-magnification SEM images of C@NiCoFe-SO_4.

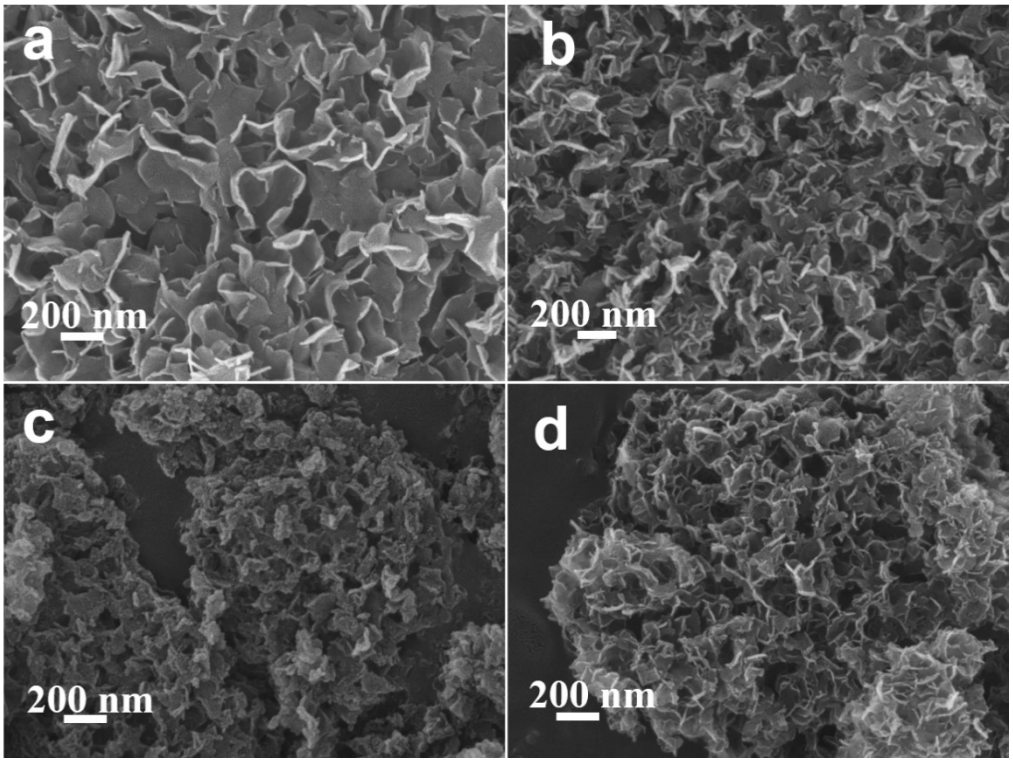

Figure S4. SEM images of (a) NiCoFe-Cl, (b) C@NiCoFe-Cl, (c) NiCoFe-OAc and (d) C@NiCoFe-OAc.

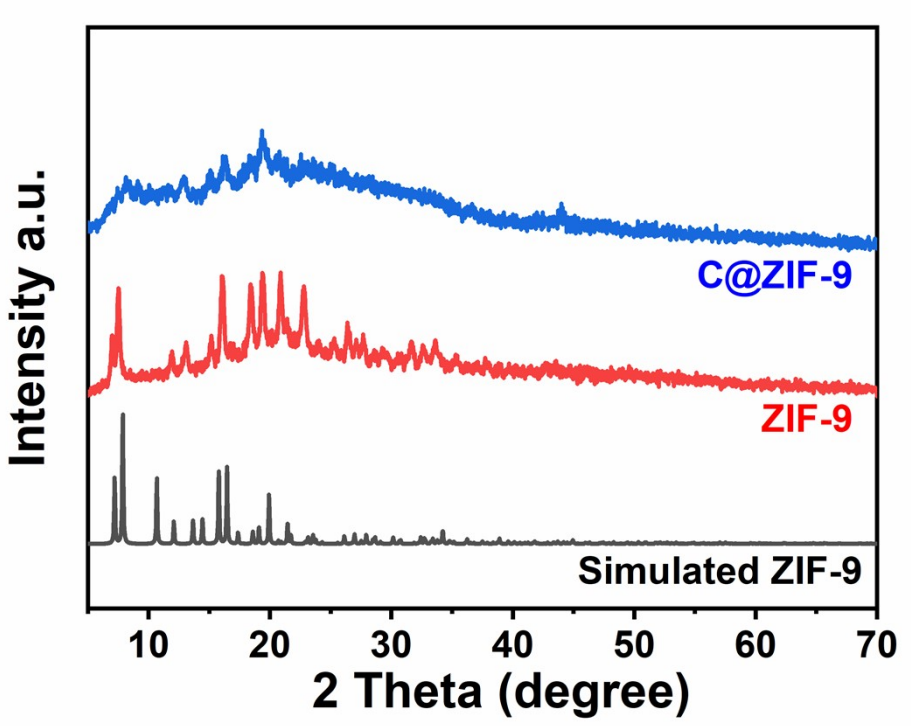

Figure S5. XRD patterns of ZIF-9 and C@ZIF-9.

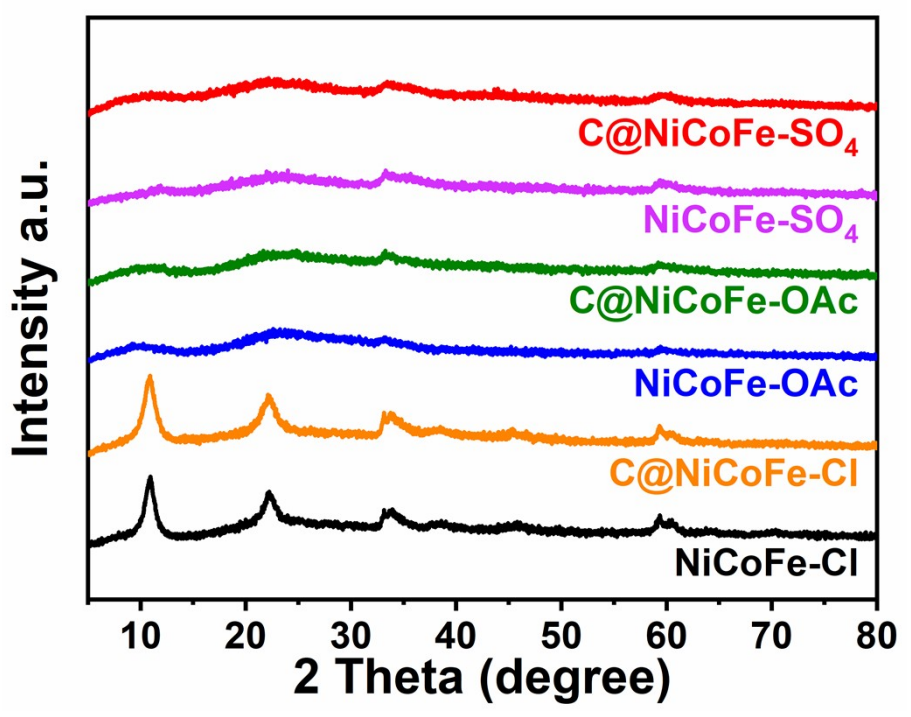

Figure S6. XRD patterns of C@NiCoFe-x and NiCoFe-x (x= SO_4, OAc, Cl).

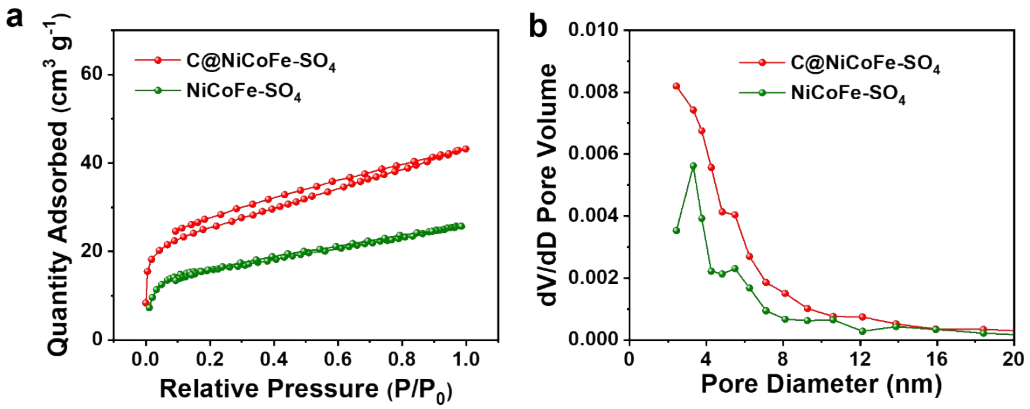

Figure S7. (a) N_2 adsorption-desorption isotherms and (b) corresponding pore size distributions of NiCoFe-SO_4 and C@NiCoFe-SO_4.

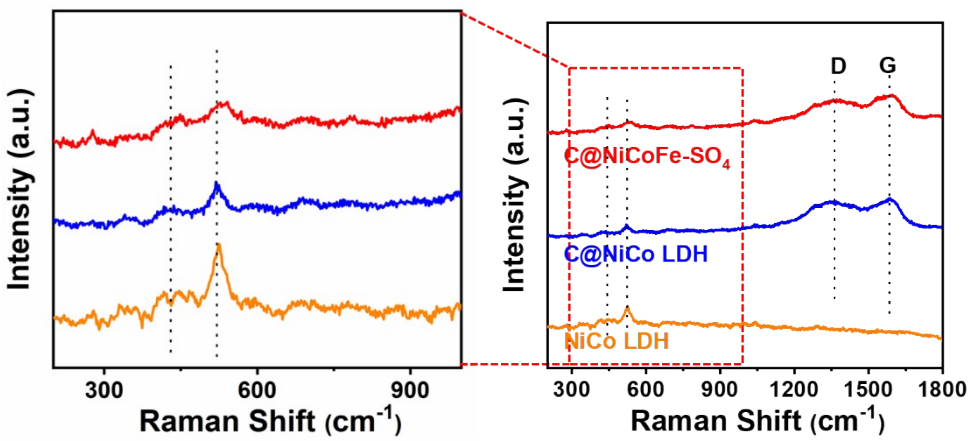

Figure S8. Raman spectra of NiCo LDH, C@NiCo LDH, and C@NiCoFe-SO_4.

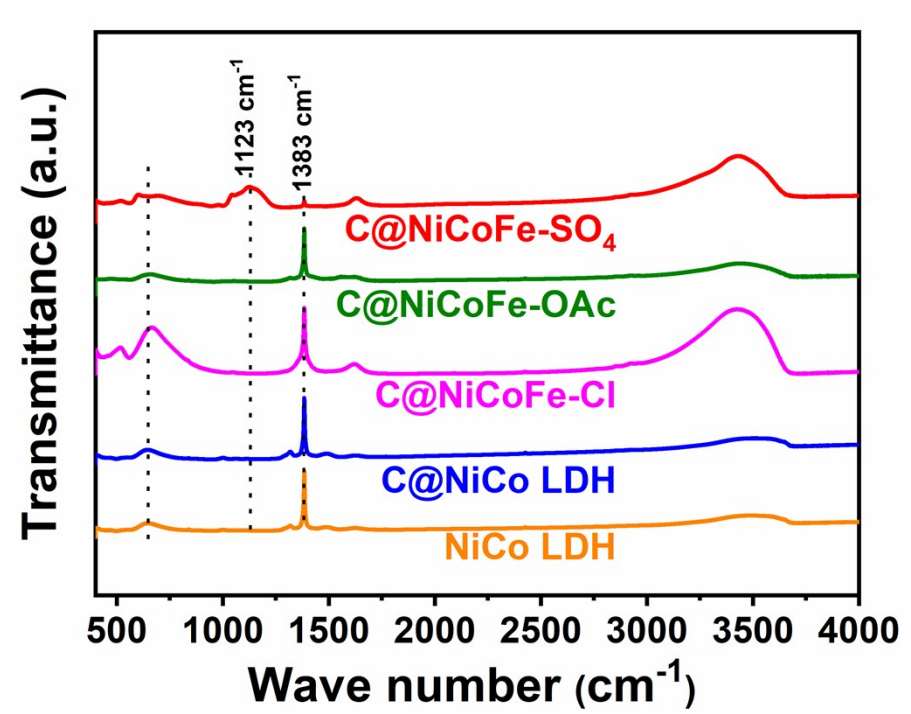

Figure S9. Fourier transform infrared spectra of NiCo LDH, C@NiCo LDH, and C@NiCoFe-x (x= SO_4, OAc, Cl).

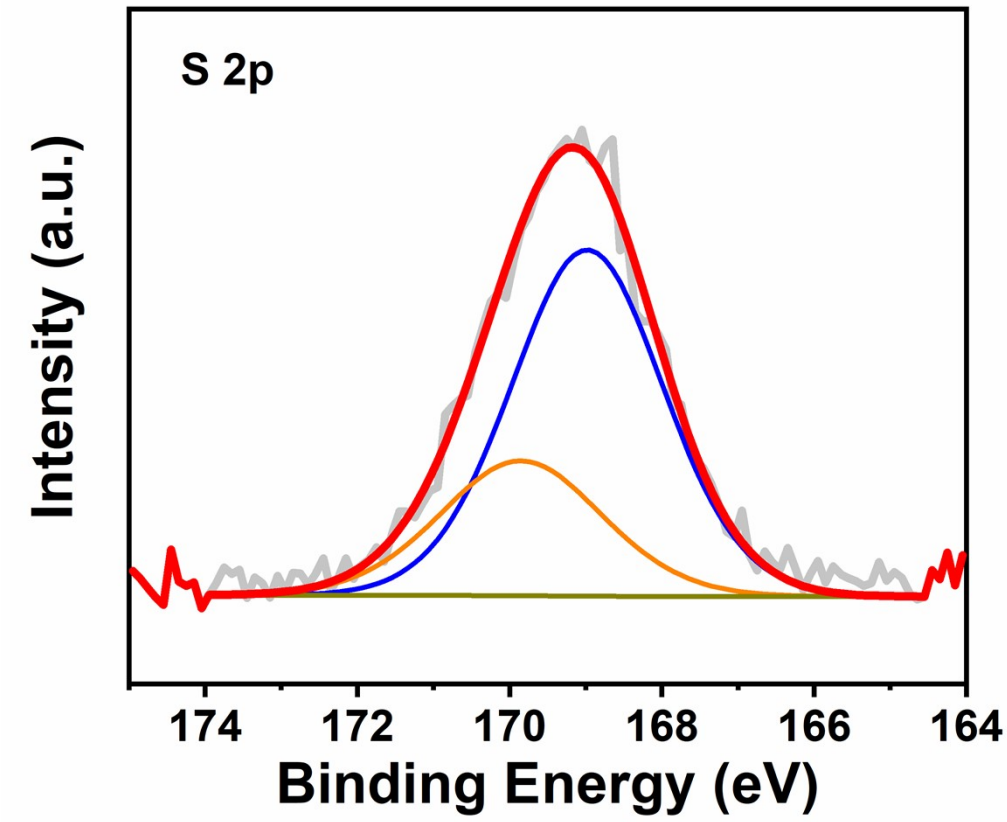

Figure S10. S 2*p* XPS of the C@NiCoFe-SO_4.

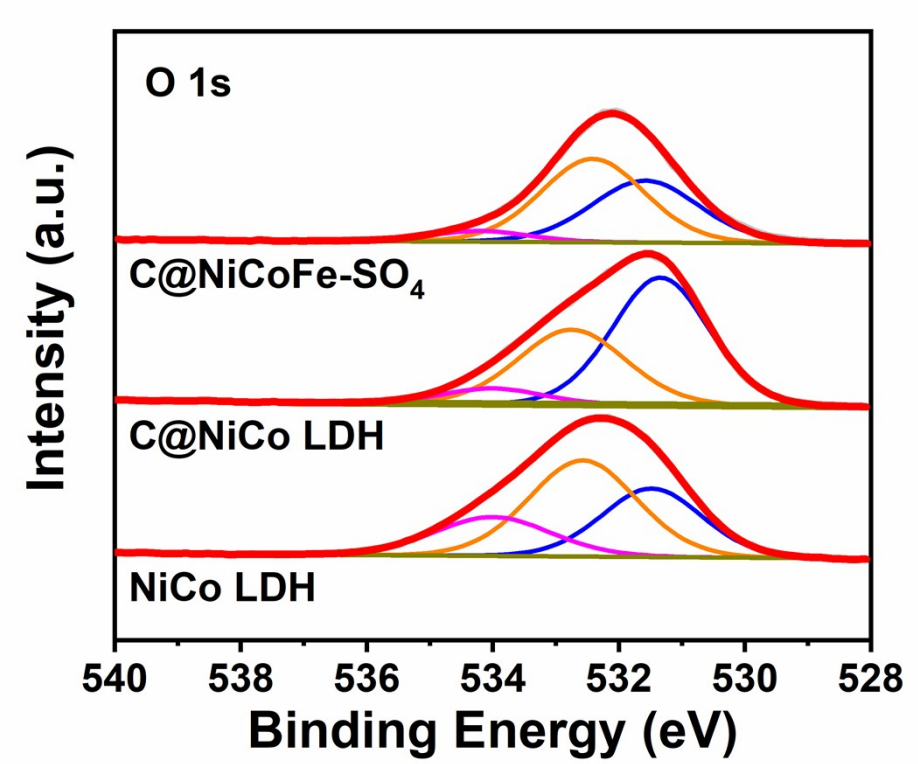

Figure S11. O 1*s* XPS of the NiCo LDH, C@NiCo LDH, and C@NiCoFe-SO_4.

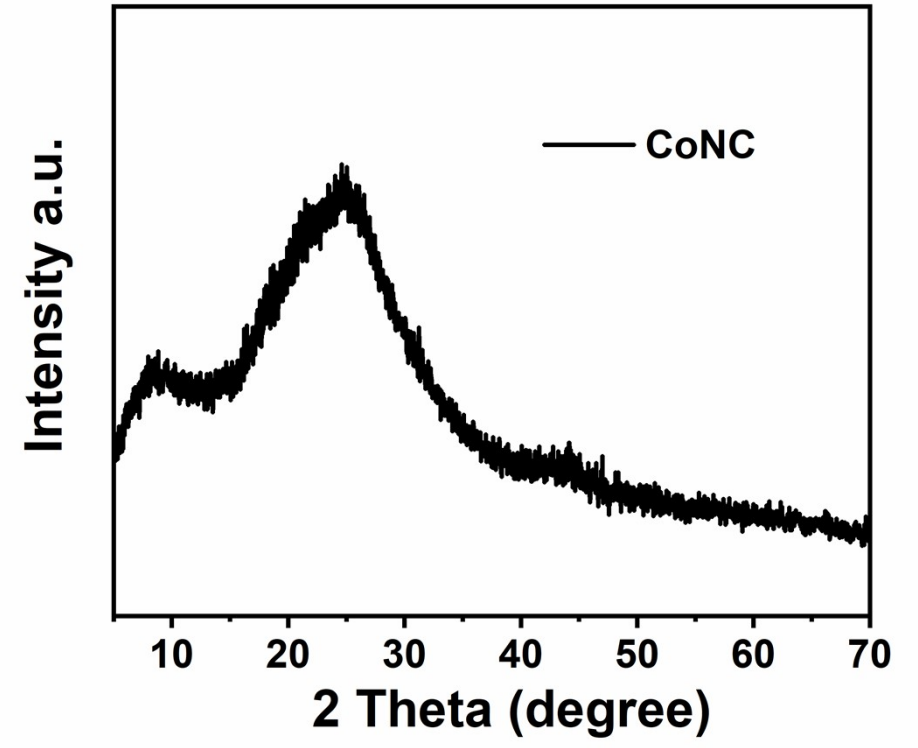

Figure S12. XRD pattern of CoNC.

CoNC was obtained through HNO_3 etching to remove the NiCoFe LDH from C@NiCoFe-SO_4.

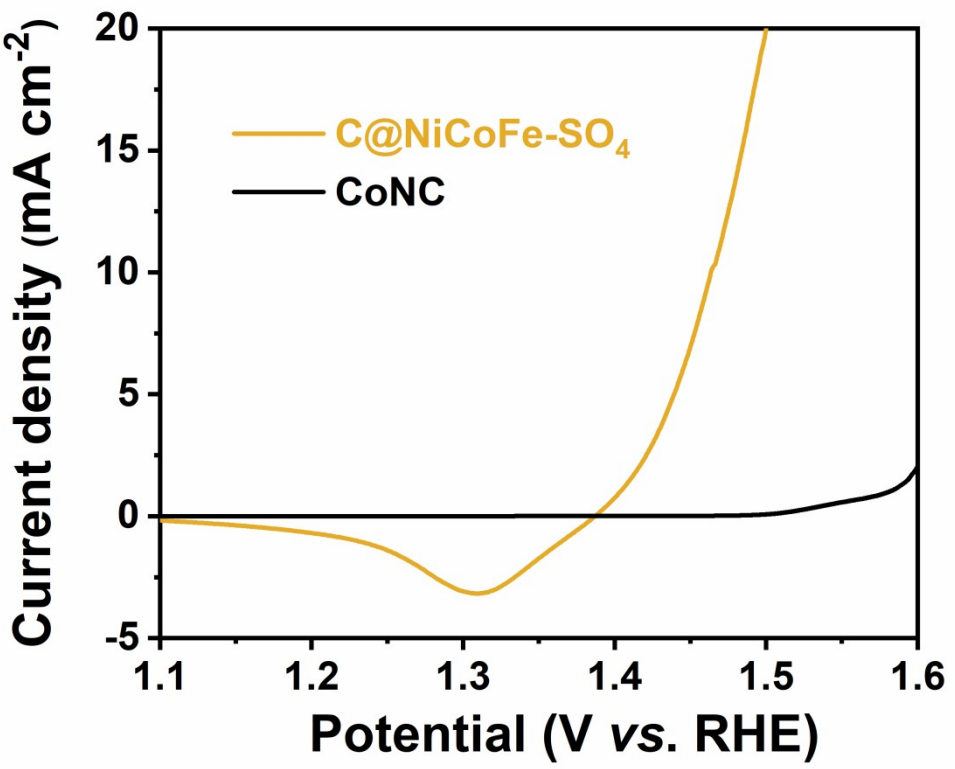

Figure S13. LSV curves of C@NiCoFe-SO_4 and CoNC.

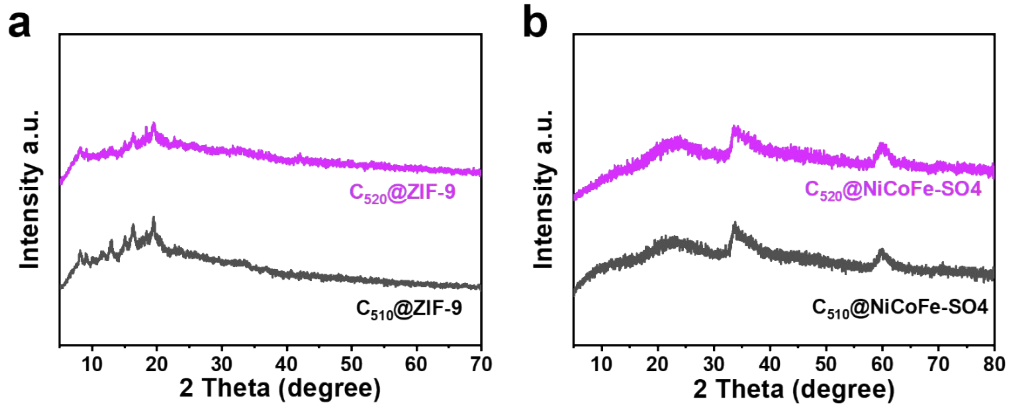

Figure S14. XRD patterns of (a) C_{510}@ZIF-9 and C_{520}@ZIF-9 prepared under a higher carbonization temperature (510 °C and 520 °C), and (b) their corresponding derived catalysts.

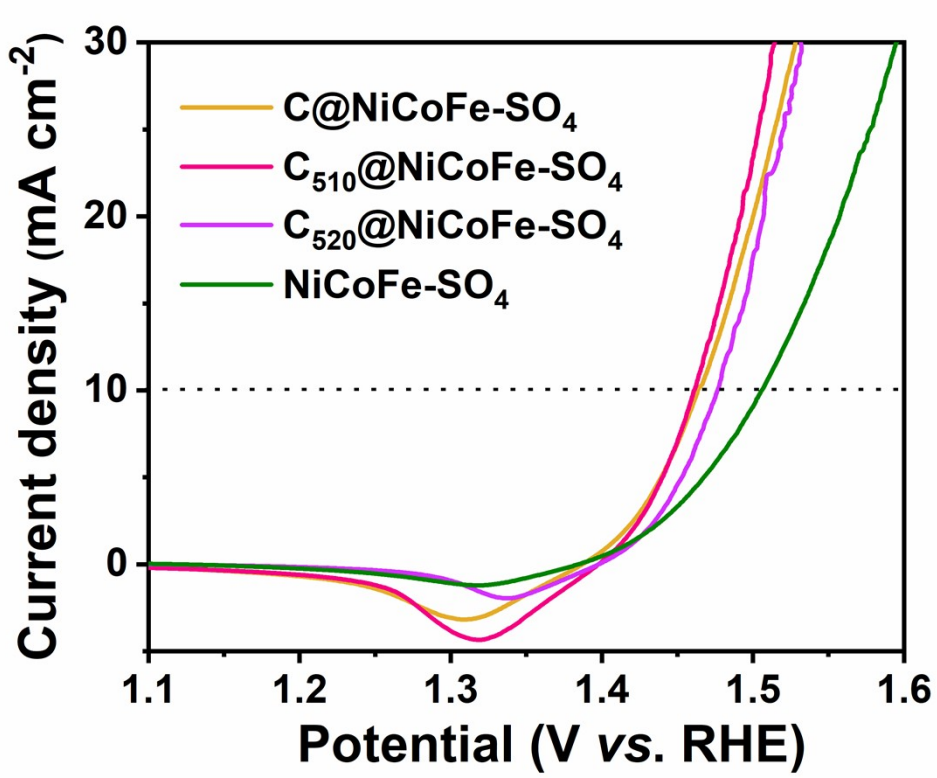

Figure S15. LSV curves of C@NiCoFe-SO_4, C_{510}@NiCoFe-SO_4, C_{520}@NiCoFe-SO_4 and NiCoFe-SO_4.

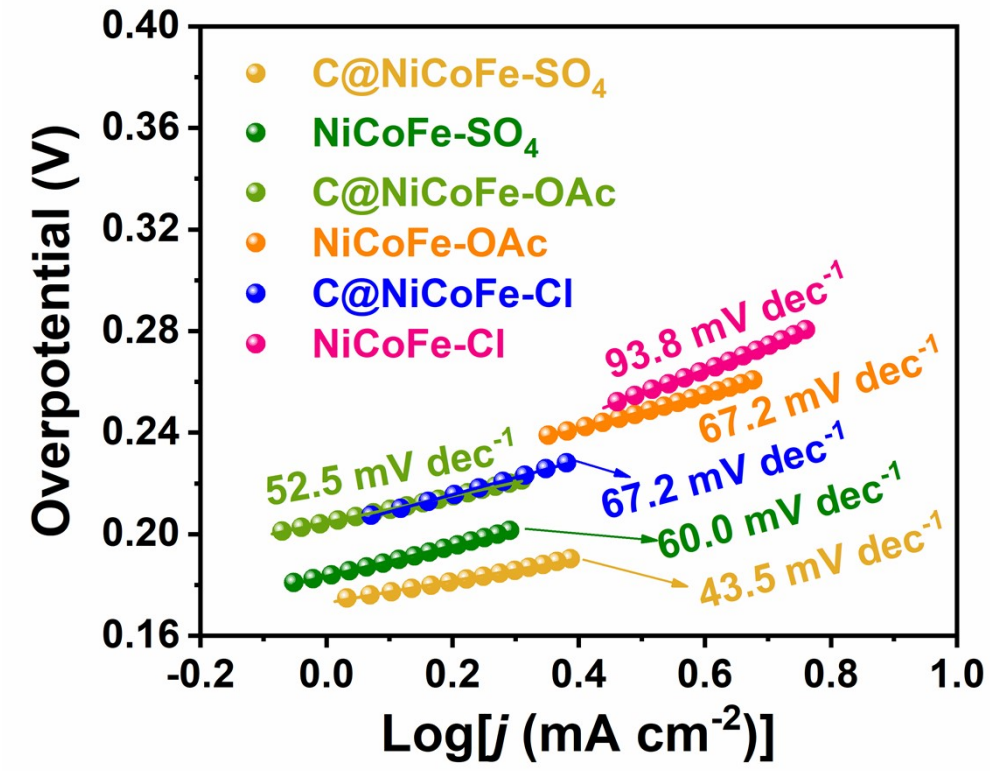

Figure S16. Tafel slope of C@NiCoFe-x and NiCoFe-x (x=SO_4, OAc, Cl) in 0.1 M KOH.

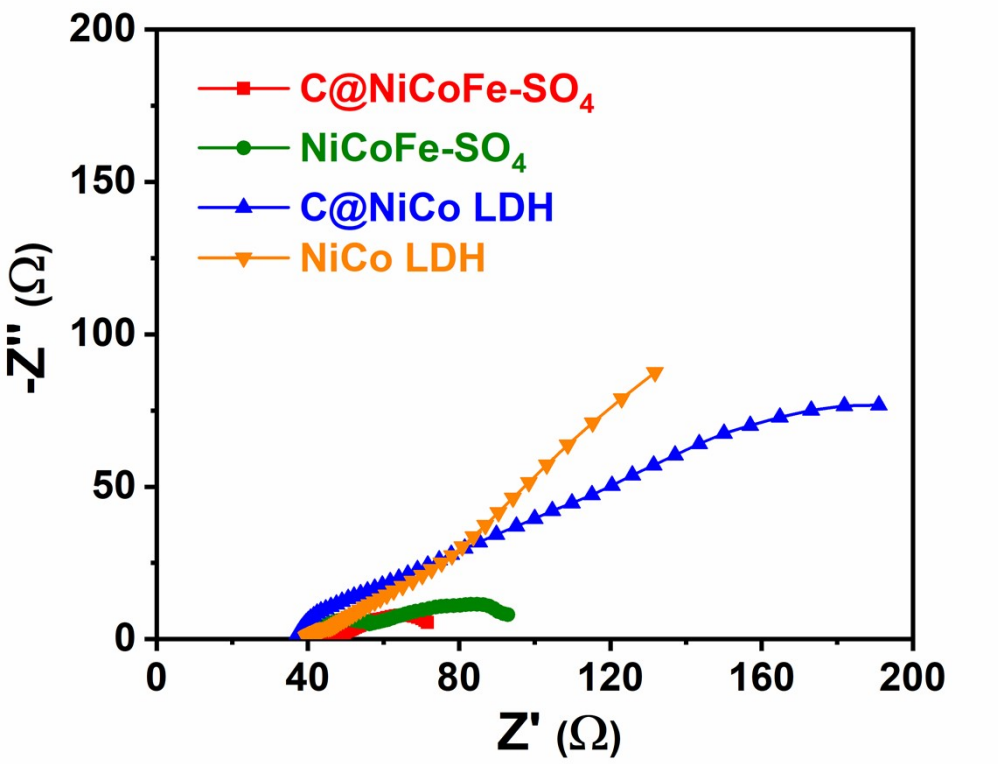

Figure S17. EIS test of the NiCo LDH, NiCoFe-SO_4, C@NiCo LDH, and C@NiCoFe-SO_4.

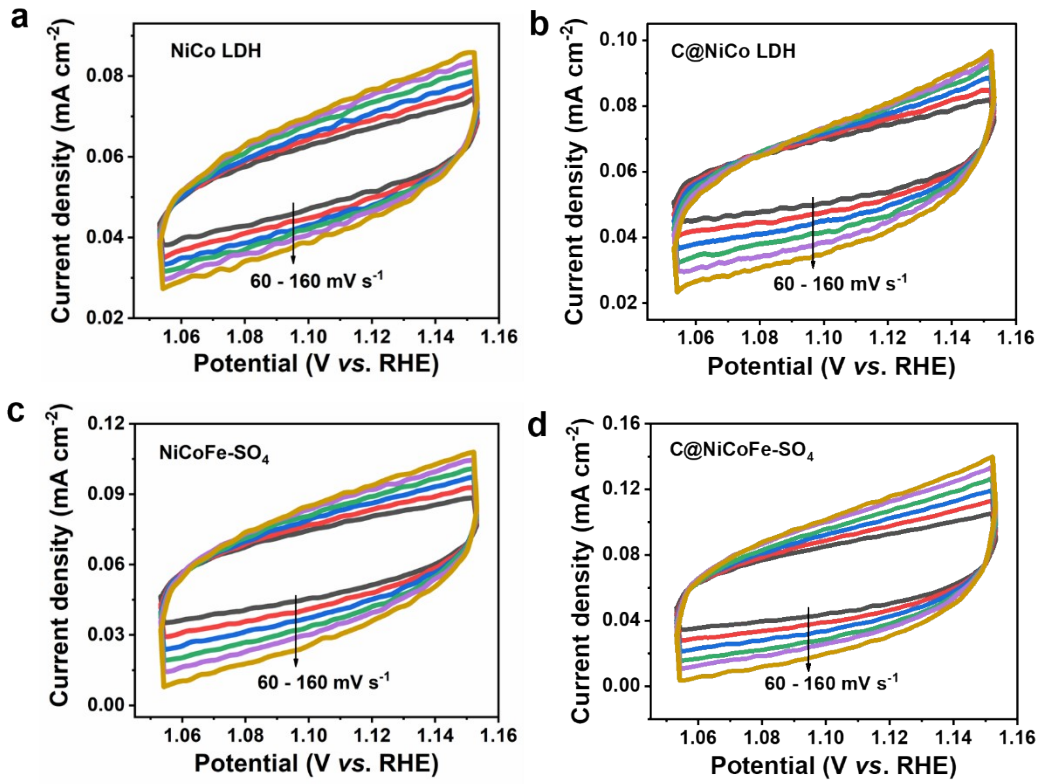

Figure S18. CVs curve of (a) NiCo LDH, (b) C@NiCo LDH, (c) NiCoFe-SO_4, and (d) C@NiCoFe-SO_4 in 0.1 M KOH for OER.

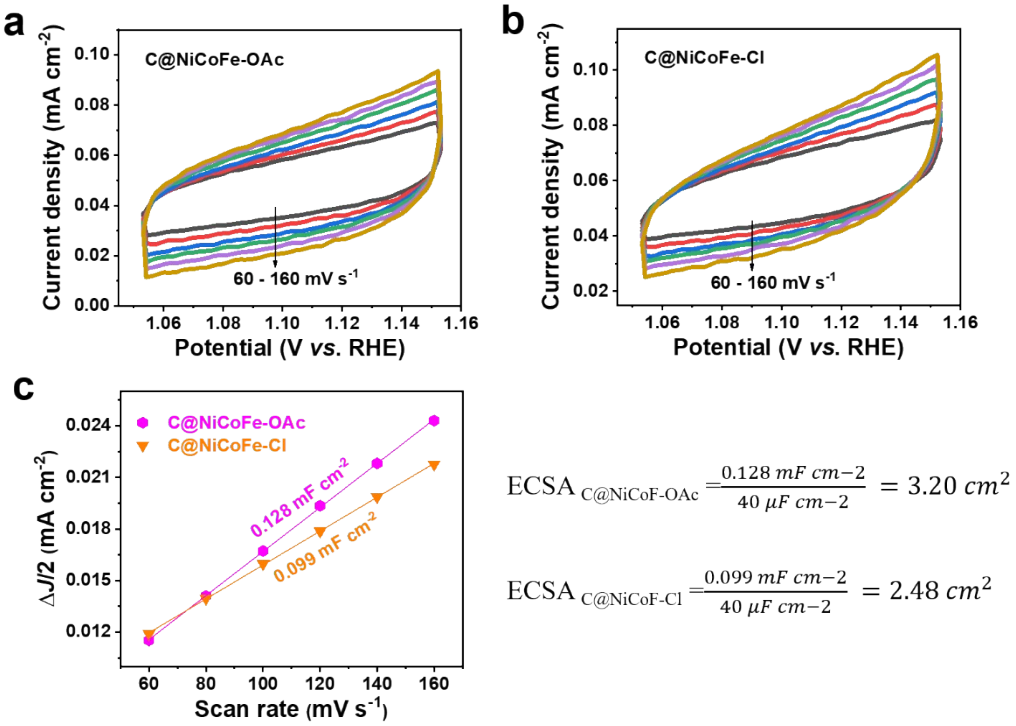

Figure S19. CVs curve of (a) C@NiCoFe-OAc, (b) C@NiCoFe-Cl, and their (c) corresponding ECSA calculation in 0.1 M KOH for OER.

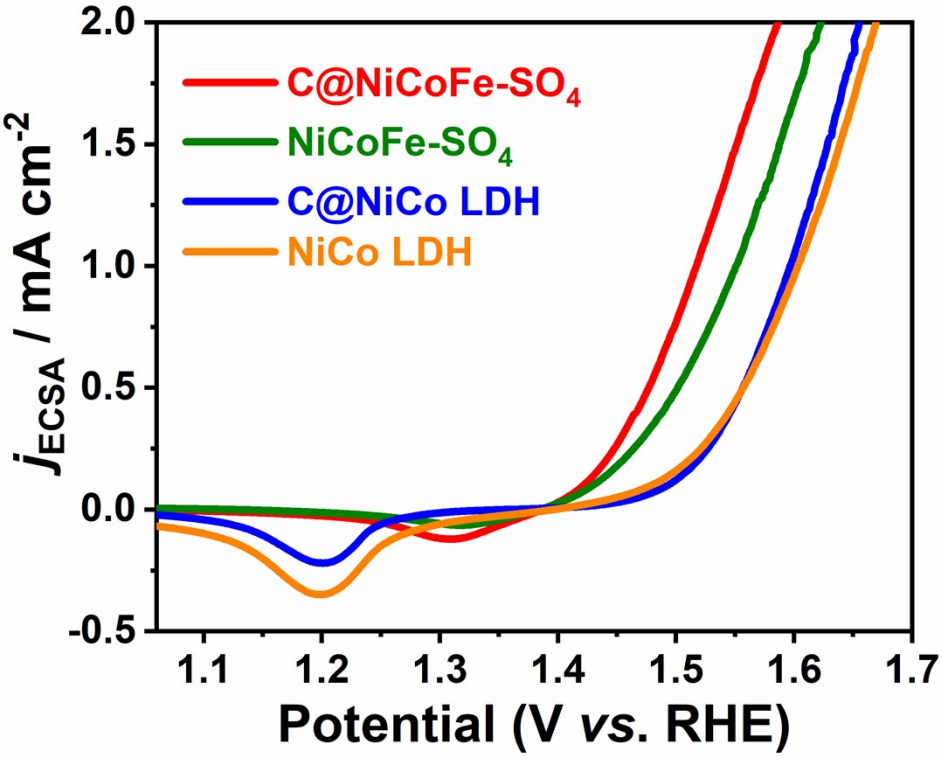

Figure S20. ECSA-normalized OER LSV curves of the NiCo LDH, NiCoFe-SO_4, C@NiCo LDH, and C@NiCoFe-SO_4.

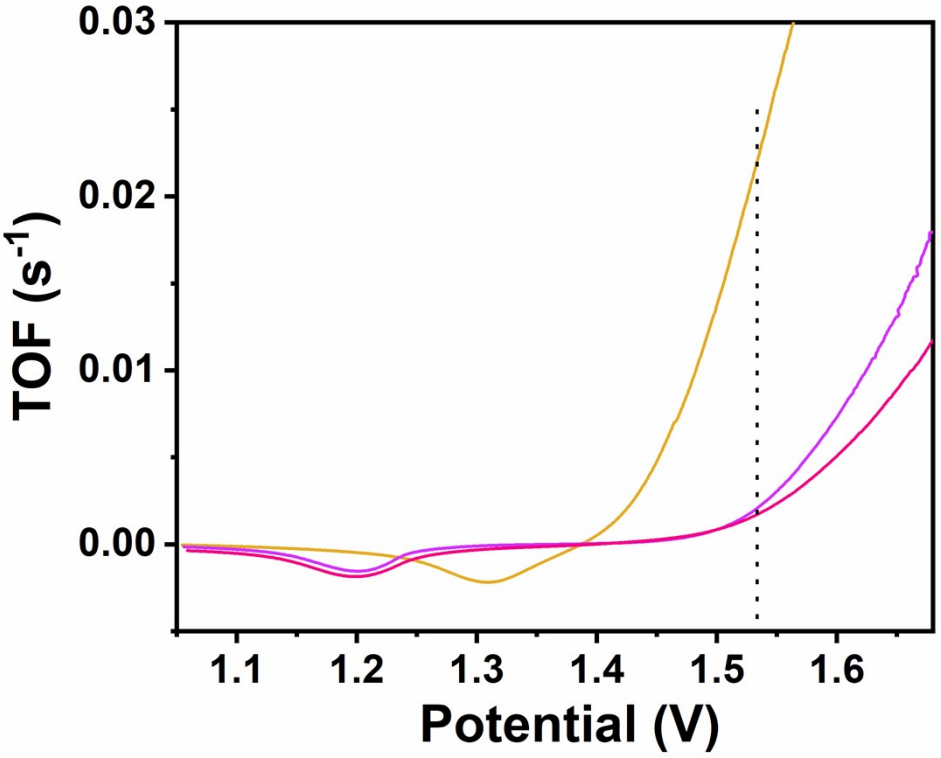

Figure S21. TOF calculation from OER.

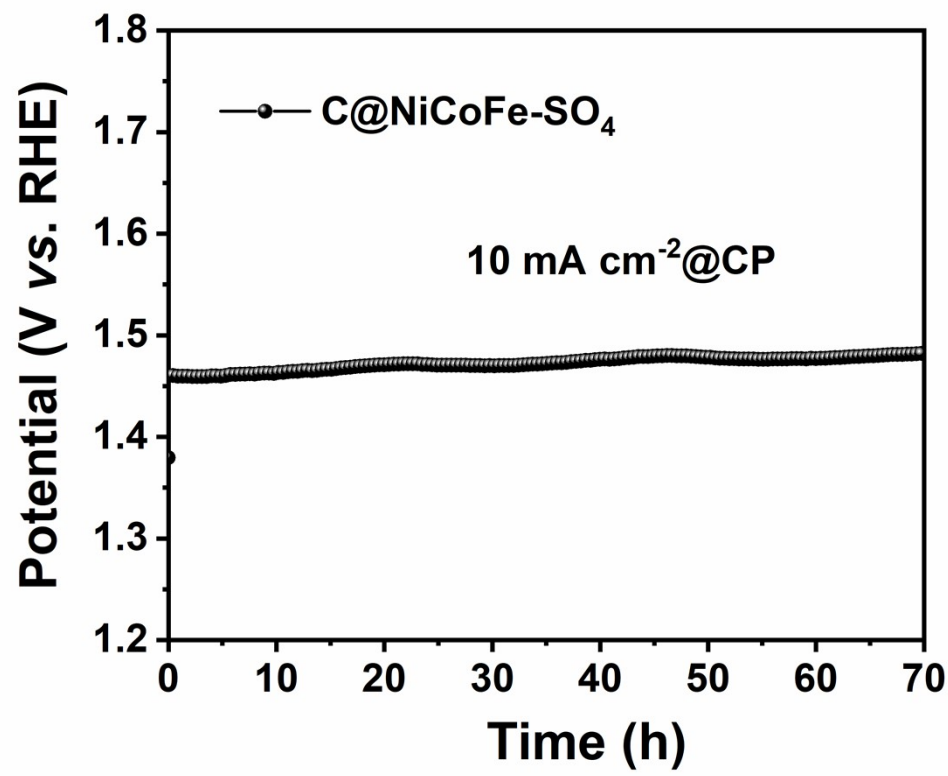

Figure S22. Chronoamperometric measurement of C@NiCoFe-SO_4 catalyst loaded on carbon parper (CP) at a current density of 10 mA cm^{-2}.

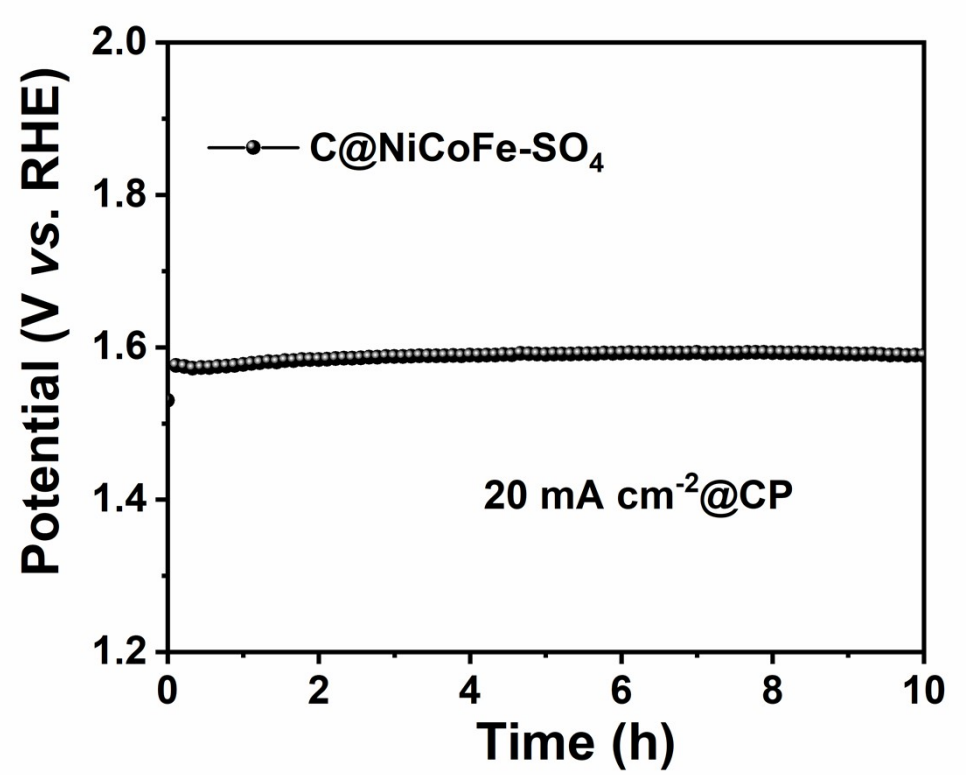

Figure S23. Chronoamperometric measurement of C@NiCoFe-SO_4 catalyst loaded on carbon parper (CP) at a current density of 20 mA cm^{-2}.

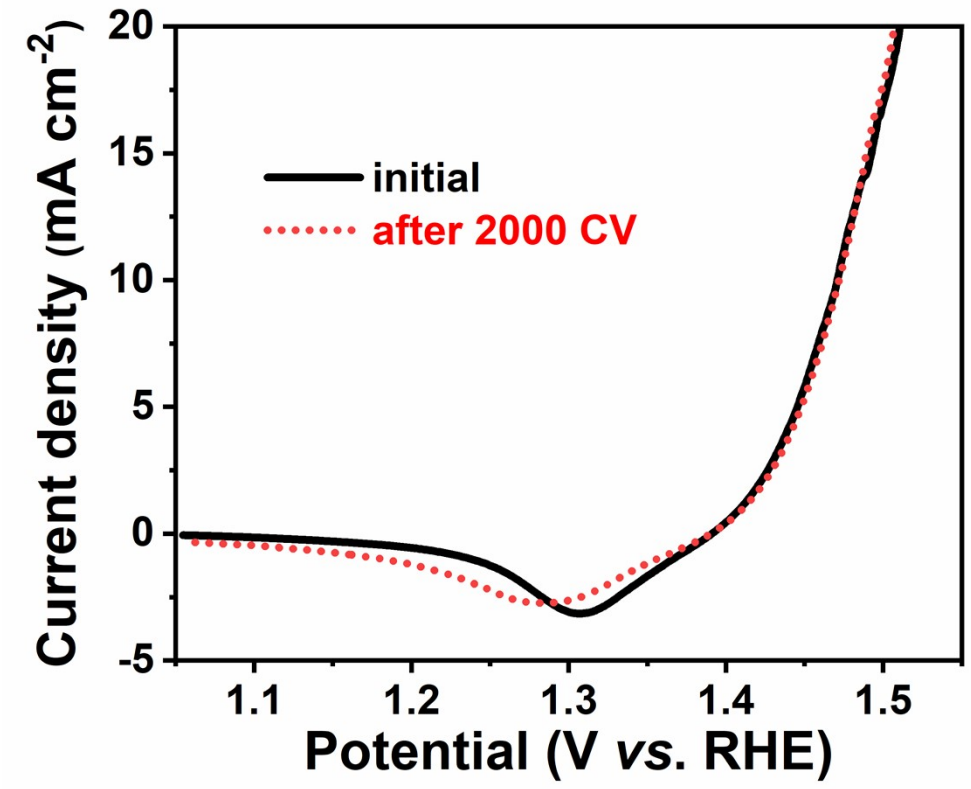

Figure S24. LSV curves of C@NiCoFe-SO_4 before and after 2000 CVs.

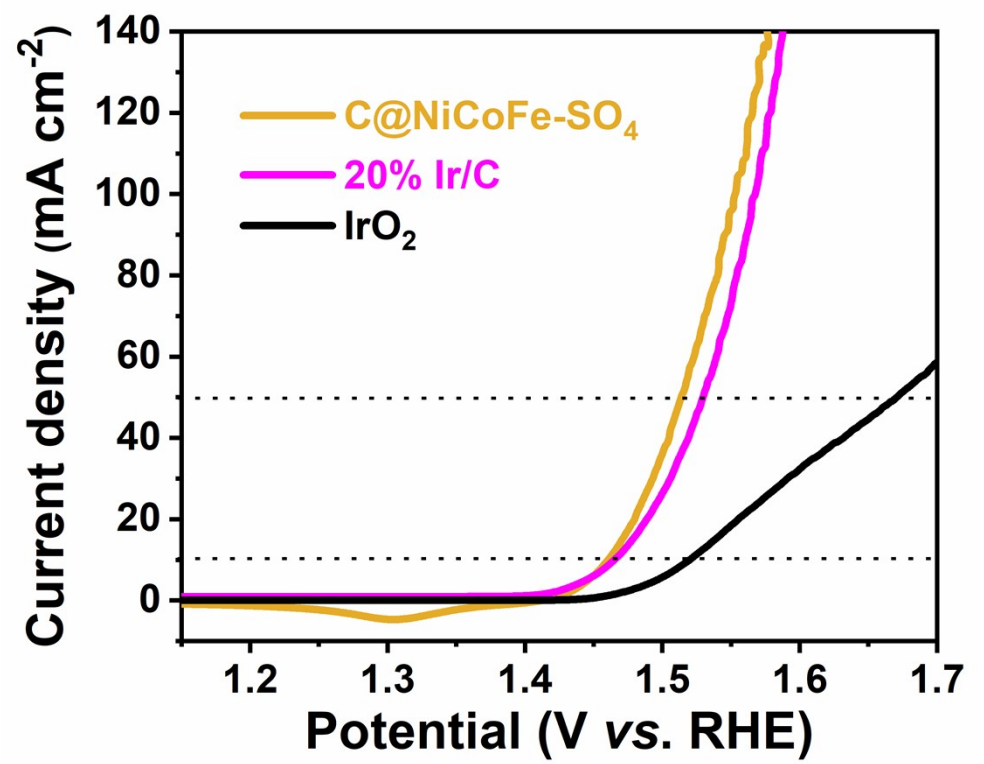

Figure S25. OER polarization curves of C@NiCoFe-SO_4, commercial Ir/C and IrO_2 with a scan rate of 5 mV/s in 1.0 M KOH medium.

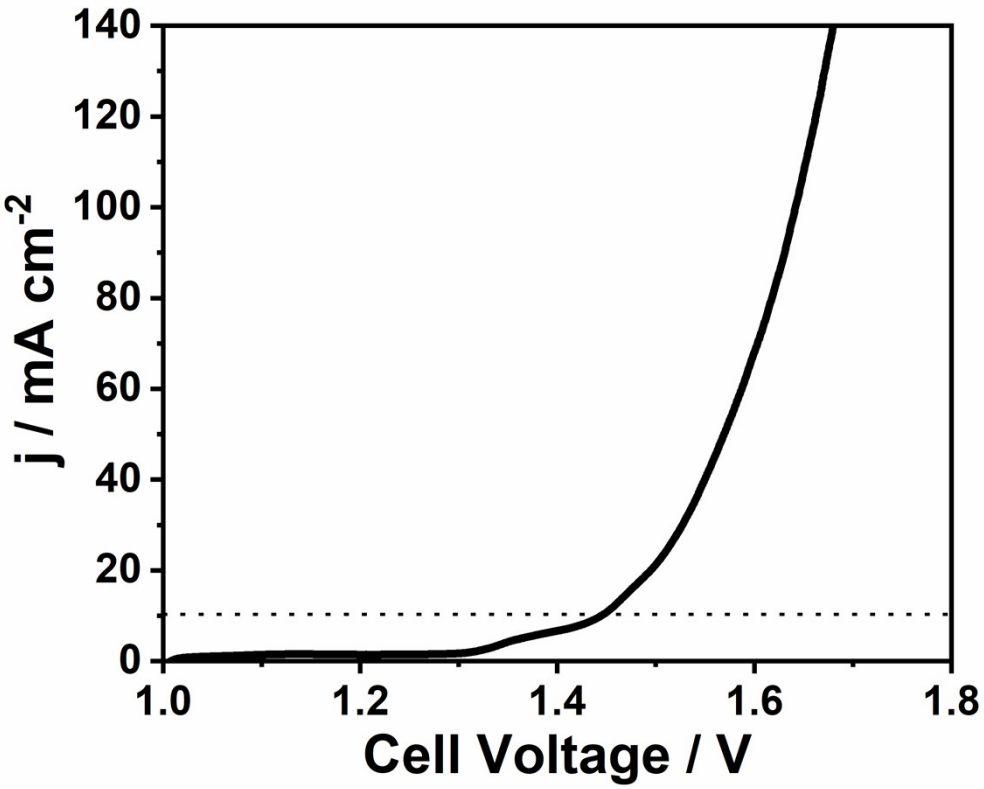

Figure S26. LSV polarization curve of the C@NiCoFe-SO_4(+)||Pt/C(–) for water

splitting in 1.0 M KOH solution.

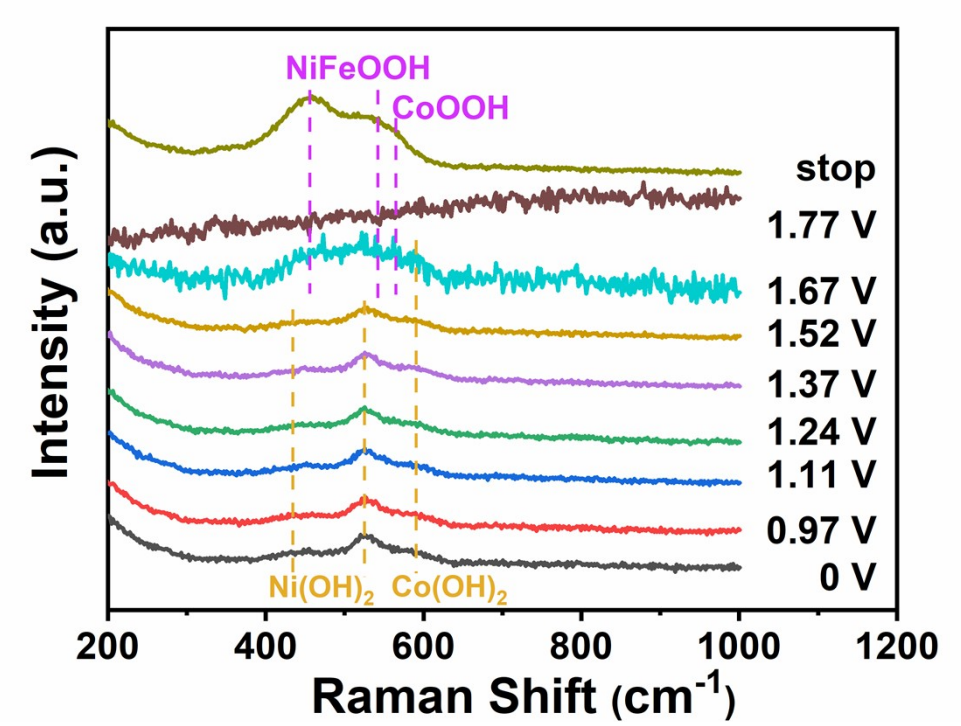

Figure S27. *In-situ* Raman spectra of C@NiCoFe-SO_4 catalyst at various applied potentials (V *vs* RHE) in 0.1 M KOH.

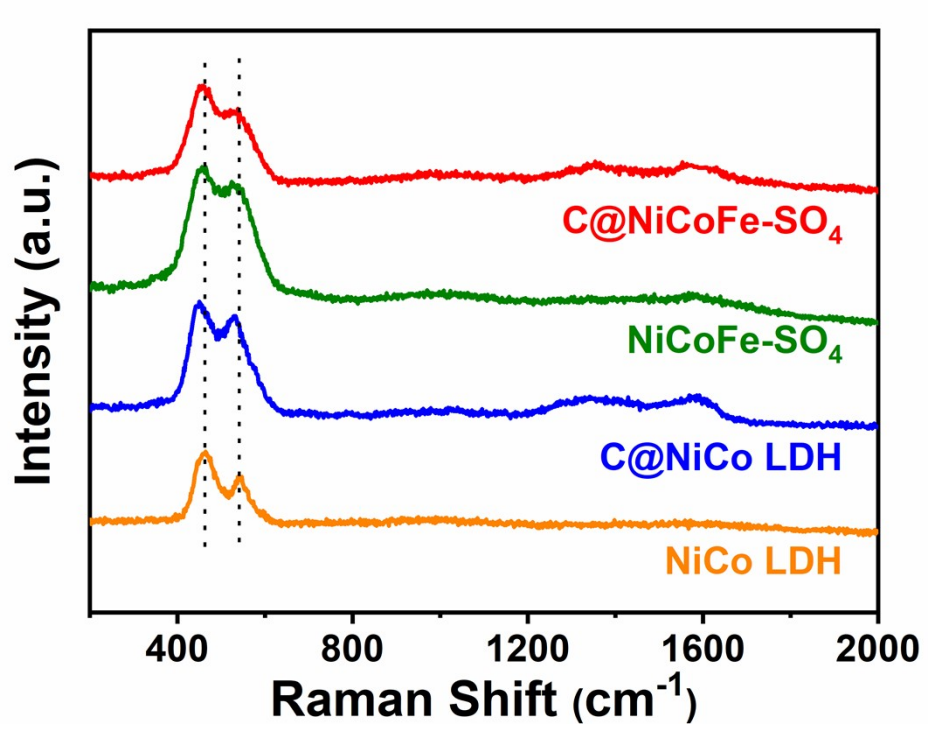

Figure S28. Raman spectra of post-OER C@NiCoFe-SO_4, NiCoFe-SO_4, C@NiCo LDH and NiCo LDH samples.

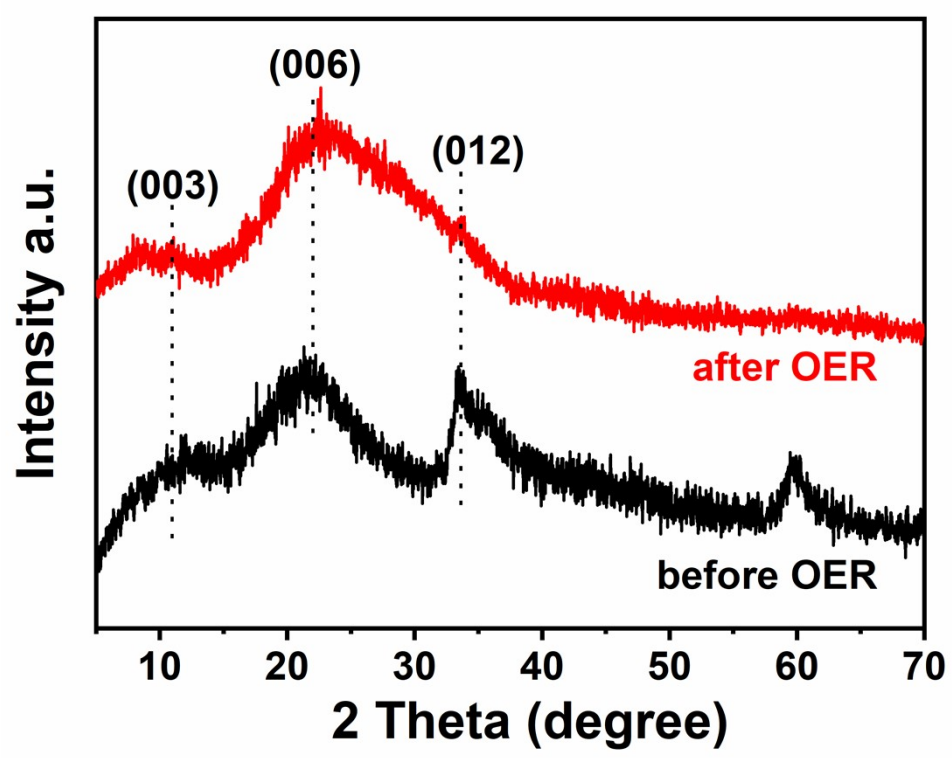

Figure S29. XRD pattern of C@NiCoFe-SO_4 before and after OER.

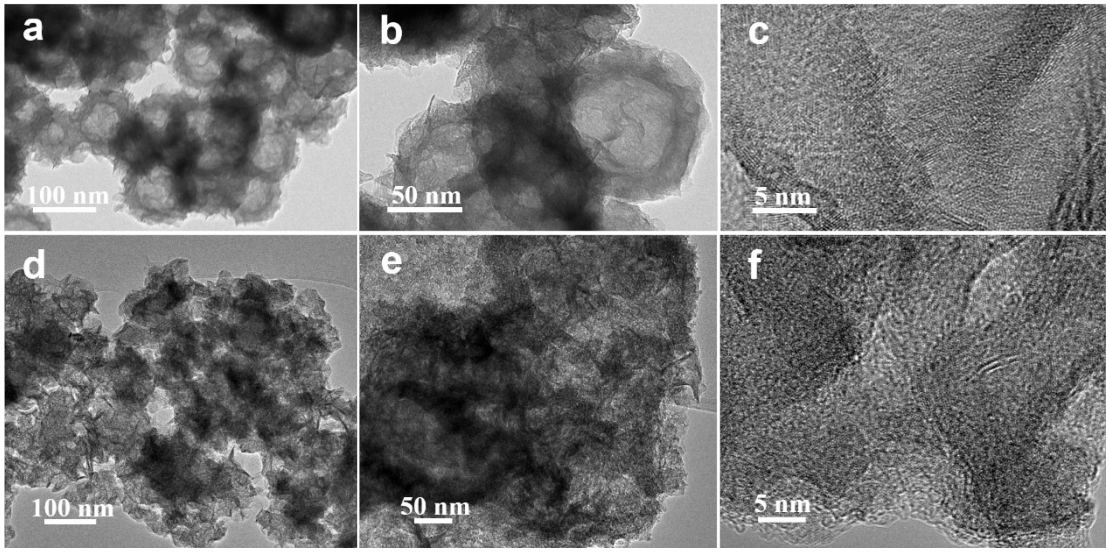

Figure S30. TEM and HR-TEM images of C@NiCoFe-SO_4 (a-c) before and (d-f) after OER.

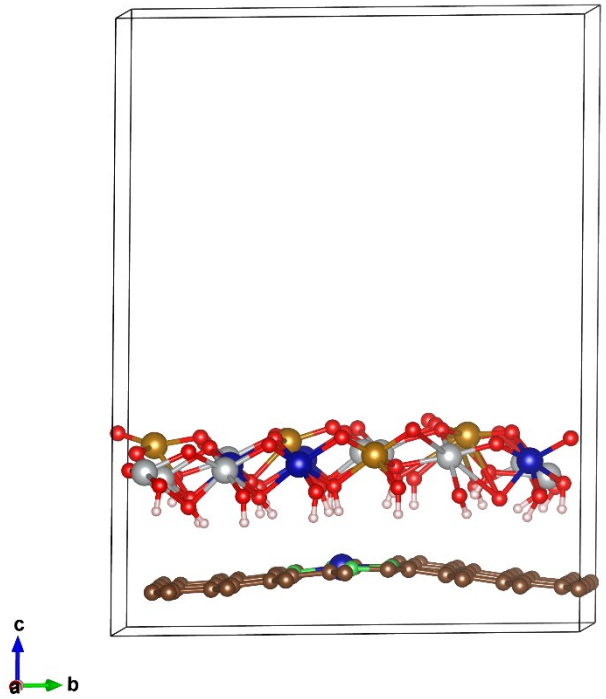

Figure S31. Optimized NiCoFeOOH/CoNC structure (H: white, C: brown, N: green, O: red, Fe: orange, Ni: silver, and Co: blue).

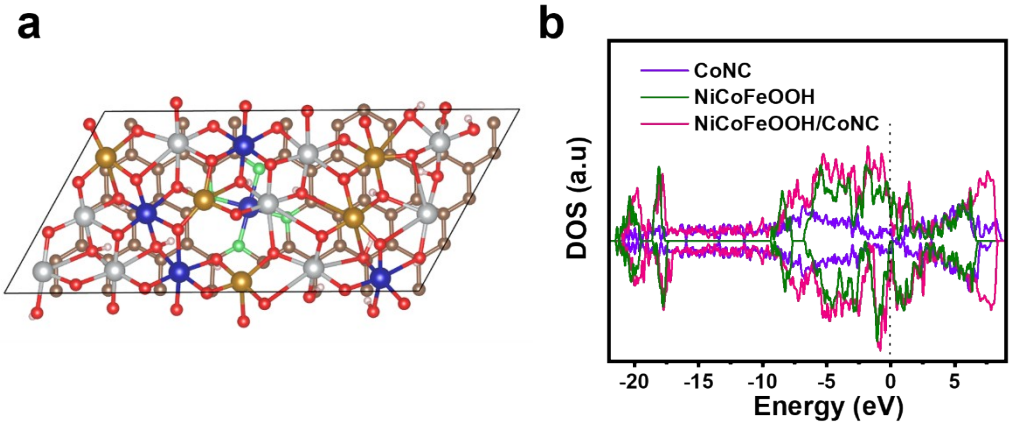

Figure S32. (a) Top view of the optimized NiCoFeOOH/CoNC composite and (b) DOS of NiCoFeOOH/CoNC, single NiCoFeOOH and CoNC with Fermi level at zero.

Table S1. Comparison of OER performance for C@NiCoFe-SO_4 with other reported transition metal-based electrocatalysts in the 0.1 M KOH.

Catalyst	Electrode	Overpotential at 10 mA cm^{-2} (mV)	Tafel slope (mV dec^{-1})	Reference
C@NiCoFe-SO_4	GCE	234	43.5	This work
FeNi@NGE/NC	GCE	372	55.2	11
Co_2-tzpa	GCE	396	88.0	12
AlOOH NFs	GCE	320	-	13
Ni_2Mo_3N	GCE	270	59	14
Fe@NG-750	GCE	275	67	15
Co-NC@LDH	GCE	389	79.65	16
$La_{0.33}SrCo_{0.5}Fe_{0.5}O_x$	GCE	260	87.8	17
CoMn-LDH/CFC-50	CFC	258	49	18
MIL-88A/$Ni(OH)_2$-CC	carbon cloth	352	46.1	19
Vs-$NiCo_2S_4$/N,S-rGO	GCE	340	65	20
CoFe/S-N-C	GCE	358	259	21
MoC/Co-N-C-600	GCE	370	59.0	22

Table S2. BET data analysis of NiCoFe-SO_4 and C@NiCoFe-SO_4 samples.

Sample	Specific Surface Area (m^2 /g)	Pore Volume (cm^3 /g)	Average Pore Size (nm)
NiCoFe-SO_4	59.8	0.0397	2.6585
C@NiCoFe-SO_4	90.0	0.0665	2.9903

Table S3. The contents of CoNC and LDH in the nanocomposites.

Catalysts	CoNC loading（wt%）	NiCoFe LDH loading（wt%）
C@NiCoFe-SO_4	20.8	79.2
C_{510}@NiCoFe-SO_4	28.1	71.9
C_{520}@NiCoFe-SO_4	35.2	64.8

A certain amount of nanocomposites (m_1) were etching using HNO_3 to remove NiCoFe LDH, and the CoNC (m_2) was obtained. Thus, the content ratio of CoNC in the nanocomposites was determined as m_2/m_1, while NiCoFe LDH was calculated as $(m_1-m_2)/m_1$.

Table S4. Loading amount of Ni, Co and Fe in NiCo LDH, C@NiCo LDH and C@NiCoFe-SO_4 samples characterized by ICP-MS.

Sample	Ni (w%)	Co (w%)	Fe (w%)	Molar ratio of Ni : Co : Fe
C@NiCoFe-SO_4	22.19	8.06	9.45	9:4:5
C@NiCo LDH	37.36	11.99	-	14:4
NiCo LDH	37.42	13.95	-	13:5

References

[1] M. Li, Y. Gu, Y. Chang, X. Gu, J. Tian, X. Wu, L. Feng, *Chem. Eng. J.*, 2021, **425**,130686.

[2] G. Kresse, J. Furthmüller, *Mater. Sci.,* 1996, ***6***, 15.

[3] G. Kresse, J. Furthmüller, *Phys. Rev. B,* 1996, **54**, 11169.

[4] J. P. Perdew, K. Burke, M. Ernzerhof, *Phys. Rev. Lett.,* 1996, **77**, 3865.

[5] G. Kresse, D. Joubert, *Phys. Rev. B,* 1999, **59**, 1758.

[6] P. E. Blöchl, *Phys. Rev. B,* 1994, **50**, 17953.

[7] S. Grimme, J. Antony, S. Ehrlich, H. Krieg, *J. Chem. Phys,.* 2010, **132**, 154104.

[8] S. Grimme, S. Ehrlich and L. Goerigk, *J. Comput. Chem.,* 2011, **32**, 1456.

[9] E. Skúlason, G. S. Karlberg, J. Rossmeisl, et al. *Phys. Chem. Chem. Phys.,* 2007, **9**, 3241.

[10] NIST Computational Chemistry Comparison and Benchmark Database, NIST Standard Reference Database Number 101, Release 21, August 2020, edited by Russell D. Johnson, III, Available at http://cccbdb.nist.gov/.

[11] S.A. Shah, Z. Ji, X. Shen, X. Yue, G. Zhu, K. Xu, A. Yuan, N. Ullah, J. Zhu, P. Song, X. Li, *ACS Appl. Energy Mater.,* 2019, **2**, 4075-4083.

[12] N. Liu, Q. Zhang, J. Guan, *Chem. Commun.,* 2021, **57**, 5016-5019.

[13] Y. Zhou, H.C. Zeng, *ACS Sustainable Chem. Eng,.* 2019, **7**, 5953-5962.

[14] Y. Yuan, S. Adimi, X. Guo, T. Thomas, Y. Zhu, H. Guo, G.S. Priyanga, P. Yoo, J. Wang, J. Chen, P. Liao, J.P. Attfield, M. Yang, *Angew. Chem. Int. Ed.,* 2020, **59**, 18036-18041.

[15] L. Bai, Z. Duan, X. Wen, J. Guan, *J. Catal.,* 2019, **378**, 353-362.

[16] D. Chen, X. Chen, Z. Cui, G. Li, B. Han, Q. Zhang, J. Sui, H. Dong, J. Yu, L. Yu, L. Dong, *Chem. Eng. J.,* 2020, **399**, 125718.

[17] H. Zhang, D. Guan, Z. Hu, Y.-C. Huang, X. Wu, J. Dai, C.-L. Dong, X. Xu, H.-J. Lin, C.-T. Chen, W. Zhou, Z. Shao, *Appl. Catal. B Environ.,* 2021, **297**, 120484.

[18] F. Yan, D. Guo, J. Kang, L. Liu, C. Zhu, P. Gao, X. Zhang, Y. Chen, *Electrochim. Acta,* 2018, **283**, 755.

[19] Z. Qian, K. Wang, K. Shi, Z. Fu, Z. Mai, X. Wang, Z. Tang, Y. Tian, *J. Mater. Chem. A,* 2020, **8**, 3311-3321.

[20] X. Feng, Q. Jiao, Q. Li, Q. Shi, Z. Dai, Y. Zhao, H. Li, C. Feng, W. Zhou, T. Feng, *Electrochim. Acta,* 2020, **331**, 135356.

[21] G. Li, Y. Tang, T. Fu, Y. Xiang, Z. Xiong, Y. Si, C. Guo, Z. Jiang, *Chem. Eng. J.,*

2022, **429**, 132174.
[22] J. Liu, Y. Guo, X.-Z. Fu, J.-L. Luo, C. Zhi, *Green Energy Environ.,* 2021. https://doi.org/10.1016/j.gee.2021.05.008.